Pergamon

Applied Geochemistry, Vol. 11, pp. 645–665, 1996

0883–2927/96 $15.00 + 0.00

PII: S0883-2927(96)00031-5

Evidence for retrograde hydrothermal reactions in near surface sediments of Guaymas Basin, Gulf of California

A. A. Sturz
University of San Diego, San Diego, CA 92110, U.S.A.

A. E. Sturdivant
California Regional Water Quality Control Board, Santa Ana Region, Riverside, CA 92507, U.S.A.

R. N. Leif
SRI International, 333 Ravenswood Avenue, Menlo Park, CA 94025, U.S.A.

B. R. T. Simoneit
Petroleum and Environmental Geochemistry Group, College of Oceanic and Atmospheric Sciences, Oregon State University, Corvallis, OR 97331, U.S.A.

and

J. M. Gieskes*
Scripps Institution of Oceanography, University of California at San Diego, La Jolla, CA 92093, U.S.A.

(*Received* 8 *July* 1995; *accepted in revised form* 23 *December* 1995)

Abstract—The Guaymas Basin, Gulf of California, is a sediment-covered portion of the East Pacific Rise, where hydrothermal fluids exit to the sea floor via both direct emanation from spires and chimneys, as well as by diffuse circulation through organic-matter-rich sediments. Thermal alteration of organic matter generates hydrothermal gas and petroleum which have wide ranges of compositions and maturities. Diffuse fluid discharge reaches the sediment/seafloor interface via channelized pathways that change with time. Mineralogical and geochemical analyses of sediments and pore fluids from an eight meter long piston core, PC 6, show superimposed geochemical signals indicating that presently active reactions are modifying previously formed authigenic materials. A slump deposit (140–250 cm) shows the presence of hydrothermal barite and a substantially changed chemical composition. Analysis of the extractable organic matter indicates that a significant amount of hydrothermally-generated oil has been transported laterally through the 140–250 cm depth interval, overwhelming the indigenous bituminous matter. Below 782 cm depth sandy layers have undergone substantial hydrothermal alteration as is evident from the presence of gypsum, dolomite, heulandite, well crystallized smectite, as well as significant changes in the bulk composition of the solid phases. The dolomite layers in the bottom part of the core act as a barrier towards upward fluid flow, allowing only diffusive communication with fluids of a hydrothermal origin. This is evident from the concentration profiles of dissolved chloride and potassium. Retrograde reactions (e.g., dissolution of gypsum), offsetting prograde hydrothermal reactions in PC 6 sediments, illustrate the ephemeral nature of fluid flow pathways in near surface Guaymas Basin sediments. Copyright © 1996 Elsevier Science Ltd

Keywords: Hydrothermal petroleum, barite, gypsum, dolomite.

INTRODUCTION

The Guaymas Basin, located at 27°N, 111.5°W, in the central Gulf of California (Fig. 1), is a site of active sea floor spreading associated with the extensional tectonics of the East Pacific Rise. New crust formed at the spreading axis is intruded into overlying sediments as sills and dikes (Einsele *et al.*, 1980; Einsele, 1982). Sediments accumulating in this shallow basin consist of hemipelagic, diatomaceous, organic carbon rich material of low density and high permeability (Curray *et al.*, 1982a). Hydrothermal alteration of sediments accompanying magmatic and sill injection activity produces hydrothermal fluids and secondary solid phases which are different in chemical and mineralogical composition than those which occur at open ocean, sediment starved spreading axes (Kastner, 1982; Kelts, 1982; Stout and Campbell, 1983; Von Damm *et al.*, 1985a, 1985b; Gieskes *et al.*, 1988; Magenheim and Gieskes, 1992). When compared to East Pacific Rise hydrothermal fluids (21°N), Guay-

* Corresponding author.

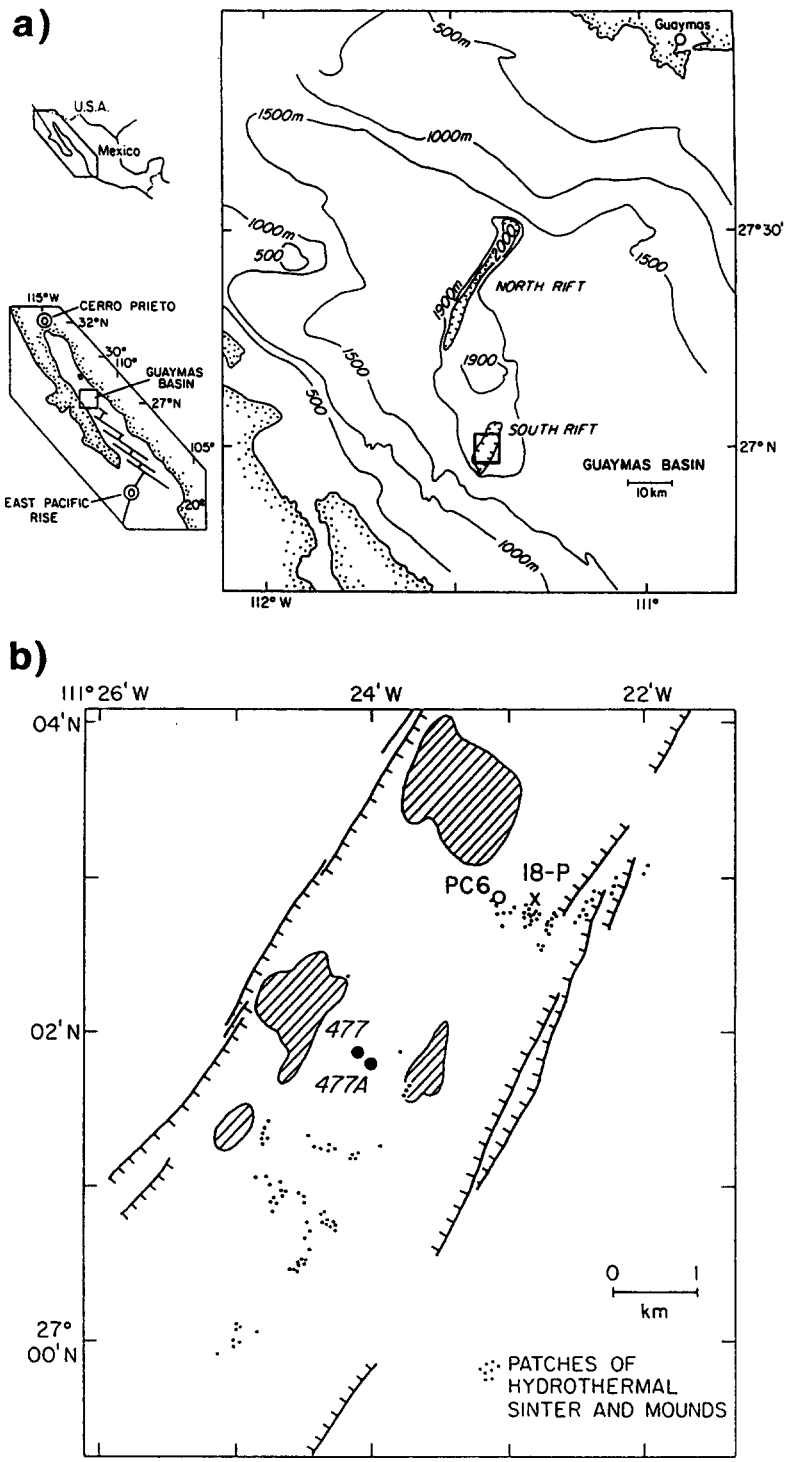

Fig. 1. (a) Index and location map of guaymas Basin. (b) Bathymetry and structure of the Southern Trough, with location of DSDP drill sites and cores PC6 and 18-P (hachured areas are slightly elevated above the rift floor).

mas basin fluids have higher pH and alkalinity, higher concentrations of H_2S, ammonium, and methane, and are depleted in dissolved metals, such as Fe, Mn, Cu and Zn (Gieskes *et al.*, 1982a; Von Damm *et al.*, 1985a, 1985b; Welhan and Lupton, 1987). Thermally enhanced diagenesis, as a result of fluid flow through the sediments, has resulted in dolomitization, the formation of pyrrhotite, anhydrite, and recrystallized clays in sediments less than 10 meters subbottom (Stout and Campbell, 1983; Magenheim and Gieskes,

1992). High thermal gradients have resulted in the direct transformation of opal-A (diatoms) to authigenic quartz (Kastner and Siever, 1983).

Based on Deep Sea Drilling Project (DSDP) Leg 64 pore water and solid phase chemical analyses, two distinct hydrothermal systems have been identified in the Guaymas Basin (Kastner, 1982; Gieskes *et al.*, 1982b). The smaller system is driven by shallow sill emplacement into low density, high porosity sediments. Fluid expulsion is observed as large reductions in porosities above and below the sills, and part of the expelled fluids rise to the surface, where they emanate directly from the sediments (Gieskes *et al.*, 1988) or they lead to the formation of hydrothermal mounds and vents (Von Damm *et al.*, 1985b). Thermal alteration of the sediments is short lived. Shallow sills cored at DSDP Site 477 were injected approximately 20,000 years ago and have cooled to ambient temperature since their emplacement (Einsele *et al.*, 1980; Einsele, 1982). Kastner (1982) described this as a closed system, which did not exceed 230–250°C, based on hydrothermal mineralogy and oxygen isotopic analyses of recrystallized calcite. Lonsdale and Becker (1985), however, suggested that recharge of bottom waters would play a role in this smaller and shallow system.

The second system is large, more deep seated, and reaches higher temperatures (Kastner, 1982). This system has a longer duration and results from major shallow magma emplacement below a sediment cover of ~ 500 m (Von Damm *et al.*, 1985b; Campbell *et al.*, 1988; Gieskes *et al.*, 1988). On the basis of oxygen isotope compositions of the solid phases (Kastner, 1982) and also on the Li concentration and Li isotope systematics of the sediments (Chan *et al.*, 1994) it is evident that this system is open, causing pervasive fluid flow through the sediments, but with vertical discharge of heated fluids (up to 300°C) along faults and fissures. Oxygen isotopic analyses of secondary silicates below 180 meters below sea floor (mbsf) indicate temperatures of formation in excess of 300°C (Kastner, 1982). The sediments in the deep seated system are altered to the hornfels facies at depths below 100 mbsf. This is documented by the presence of the mineral assemblage quartz–albite–chlorite–epidote which occurs in altered sediments of DSDP Site 477 (Kastner, 1982; Kelts, 1982). Magenheim and Gieskes (1992) describe the hydrothermal discharge in the form of disperse fluid flow from the sediments and the associated alteration of surface sediments.

Detailed heat flow studies have been carried out in the entire Guaymas Basin, but with particular attention to the Southern Rift zone (Southern Trough), the area under consideration in this paper. Fisher and Becker (1991) have summarized this information and delineated several modes of heat transfer in both troughs of the basin. A combination of deep conductive heat flow, slow intergranular fluid circulation, and vigorous hydrothermal venting leads to broad heat flow highs of several square kilometers in area. The area with the highest heat flow is around the northern vent field of the Southern Trough, where heat flow values higher than 1000 mW/m^2 were recorded.

Petroleum products are generated instantaneously on a geological time scale (decades to millennia) as a consequence of hydrothermal processes (Simoneit and Lonsdale, 1982; Simoneit, 1983a, 1983b, 1985). This petroleum generation and migration occurs by both sustained high heating of immature, unconsolidated sediment by an inferred magma chamber at depth and by dike and sill intrusions into these sediments (Simoneit, 1983a, 1983b, 1984, 1985; Simoneit *et al.*, 1984, 1992). Thus, both localized heating and the high thermal gradient pyrolyze the sedimentary organic matter to petroleum products ranging from methane to asphalt. The hydrothermal oils from the seabed in Guaymas Basin were sourced at shallow subbottom depth (12 – 30 mbsf, Simoneit and Kvenvolden, 1994) and have migrated as solutions, emulsions, or bulk phase to the seafloor, where the volatiles vented and the heavy oil solidified. These hydrothermal petroleums have similar bulk compositions as conventional crude oils (Simoneit, 1983a, 1983b, 1985; Didyk and Simoneit, 1989, 1990).

This paper reports the results of mineralogical and chemical analyses of near surface sediments from an eight meter long piston core, PC 6, located at 27°02.88"N, 111°23.24"W in the Southern Trough (Fig. 1b) at the edge of a high heat flow zone, but in the vicinity of hydrothermal vents. The sediments show evidence of hydrothermal alteration in their mineralogy, gas chemistry, and the occurrence of hydrothermal oils (Simoneit *et al.*, 1992). Detailed studies of the hydrothermal components indicate that retrograde reactions may affect these sediments. The evidence for hydrothermal alteration of solid phases from core PC 6 is compared with evidence for such alteration in the chemical composition of the pore waters. The volatile hydrocarbon signatures and the yields and molecular compositions of the extractable organic matter of PC 6 provide information about the thermal history of the sediment. Core PC 6 is located in the vicinity, less than 1 km, from piston core 18-P (Fig. 1b) which was shown to be undergoing active hydrothermal alteration (Stout and Campbell, 1983).

METHODS

Interstitial waters were retrieved onboard ship by high speed centrifugation. Analysis for major constituents (Cl, Ca, Mg) were carried out by titration, sulfate by nephelometry, ammonium by colorimetry, and potassium by atomic absorption techniques (Gieskes *et al.*, 1991).

The solid phases were analyzed mineralogically and texturally by standard petrographic and x-ray diffraction (XRD) techniques and by scanning electron microscopy with an electron dispersive system (SEM–EDS). XRD peak shape and height were used as semi-qualitative indicators of relative degree of crystallinity for the same mineral at various depths

in the core. Chemical analyses of the bulk sediments were carried out by fluxed fusion at 1000°C, dissolution in 0.5 M H_2SO_4 and standard atomic absorption (magnesium, calcium, potassium, iron) and colorimetric (aluminum, titanium, silica) techniques (Donnelly, 1980; Brown, 1988). Mg, K, Fe, Al, Ti, and Si concentrations for bulk sediment at four selected intervals were also determined by x-ray fluorescence (Sturdivant, 1988), mostly to serve as a check on the above wet chemical analyses.

Exchangeable and fixed ammonium were determined in the bulk sediments by ion chromatography, following distillation to extract exchangeable ammonium and fusion decomposition to extract fixed ammonium (Sturdivant, 1988). Organic carbon and any associated nitrogen were removed by low temperature oxygen plasma ashing at 60°C prior to ammonium extraction. This removal eliminates the potential for anomalous ammonium values from nitrogen contributed during breakdown of organic molecules.

Stable oxygen and carbon isotopes were determined by mass spectrometry of the CO_2 from the phosphoric acid–CO_2 liberation technique of McCrea (1950).

Clay mineralogy was determined by settling to retain the $<2\mu m$ fraction and XRD analyses of the untreated, glycolated and heat treated (525°C) 001 and 060 reflections.

Organic carbon contents and ratios of hydrocarbon and CO_2 to organic carbon, Hydrogen Index and Oxygen Index were determined by Rock–Eval pyrolysis (Sturdivant, 1988). Rock–Eval is an analytical procedure for rapid characterization of petroleum source rocks based on pyrolysis of bulk sediments (Espitalié *et al.*, 1977, 1986).

The volatile hydrocarbons in the headspace of the sealed samples were analyzed by sub-ambient capillary gas chromatography (GC) on board ship (Simoneit *et al.*, 1988, 1992). The GC column oven was cryogenically cooled with liquid CO_2 at the beginning of each analysis. The soluble organic matter was obtained by methylene chloride/methanol extraction using multiple ultrasonication (typically 3–5 times), followed by deasphalting, then liquid–solid column chromatography and analysis by GC and gas chromatography–mass spectrometry (GC–MS) (Kawka and Simoneit, 1987; Simoneit *et al.*, 1992).

RESULTS

Core description

Core PC 6 consists mostly of fine grained, very dark grayish to greenish brown mud (Fig. 2). Based on quantitative settling according to Stokes Law of 23 intervals throughout the core, sediments recovered in PC 6 contain about 50% clay size materials. Textural differences between the 140–250 cm interval and sediments above and below suggest that this interval probably represents semi-consolidated sediments, which were disrupted and redeposited as a debris flow. This interval is bounded at the top and bottom by relatively more indurated layers (Fig. 2). The upper layer is 0.5 cm thick, and the lower is 1 cm thick. The two bounding layers are breccias, containing angular fragments of indurated greenish brown clay in a less indurated matrix of dark grayish brown silty clay. Between the two breccias is a zone of dark brown to greenish brown silty clay. Below 782 cm the sediment is characterized by the occurrence of silty sand with dolomite layers. Petrographic observations of thin sections of the sediments between 140 and 250 cm and of the lower sand layer, set in epoxy and thin sectioned, indicate void space of 30–40%, much lower than the surrounding sediment.

Though minor amounts of illite and kaolinite are present in most intervals, smectite dominates the clay mineral assemblage (Table 1). Smectite crystallinity increases with depth in the core, at considerably shallower depths than would be expected from normal burial diagenesis (e.g., Hower *et al.*, 1976, Eberl *et al.*, 1978; Velde and Nicot, 1985). Heulandite is present throughout the core, but its abundance increases below 780 cm (Table 2). Barite occurs noticeably in the upper debris flow unit (140–250 cm), but also to some extent below 790 cm. The distribution of these minerals is presented in Fig. 3.

Gypsum and dolomite are present below 783 cm depth (Table 2). Calcium sulfate (as anhydrite) and dolomite were also observed by Stout and Campbell (1983) in core P-18 sediments where thermally enhanced diagenesis is presently active. Based on petrographic inspection and SEM analyses, sediments in PC 6 are diatom bearing, but well preserved diatoms make up less than 1% of the biogenic phases. Diatoms are abundant in unaltered Guaymas Basin sediments (Curray *et al.*, 1982a), but are susceptible to dissolution by heated fluids (Kastner and Siever, 1983). The presence of hydrothermal minerals at very shallow levels and the absence of diatoms indicates that large sections of the sediments in core PC 6 have been subjected to hydrothermal alteration.

Stable isotopic analysis of oxygen and carbon of the dolomite allows an estimate of the temperature of formation as demonstrated by Epstein *et al.* (1953). The latter authors provided an equation which requires the measured oxygen isotope ratio of the dolomite ($\delta^{18}O = -7.02‰$/SMOW) and the oxygen isotope ratio of the fluid from which the dolomite formed. The oxygen isotope ratio of the interstitial water used for these calculations ranges from the sea water value to the value obtained by Gieskes *et al.* (1982a) in Guaymas Basin Site 481 (0 to +3‰/SMOW). Thus, the estimated temperature of formation of the dolomite is then between 54 and 73°C. The measured carbon isotope ratio of the dolomite ($\delta^{13}C = -14.31‰$ PDB) indicates a significant source (up to 50%) from the decomposition of sedimentary organic matter (cf., Kelts and McKenzie, 1984).

Mineralogy

Mineralogical evidence supporting enhanced hydrothermal alteration within the 140–250 cm depth interval includes the presence of authigenic smectite and barite, and the absence of calcite within this unit. Though illite and kaolinite are present in adjacent intervals, smectite makes up 100% of the clay mineral fraction between 204 and 251 cm depth. Barite is present in PC 6 within the unit bounded by the two

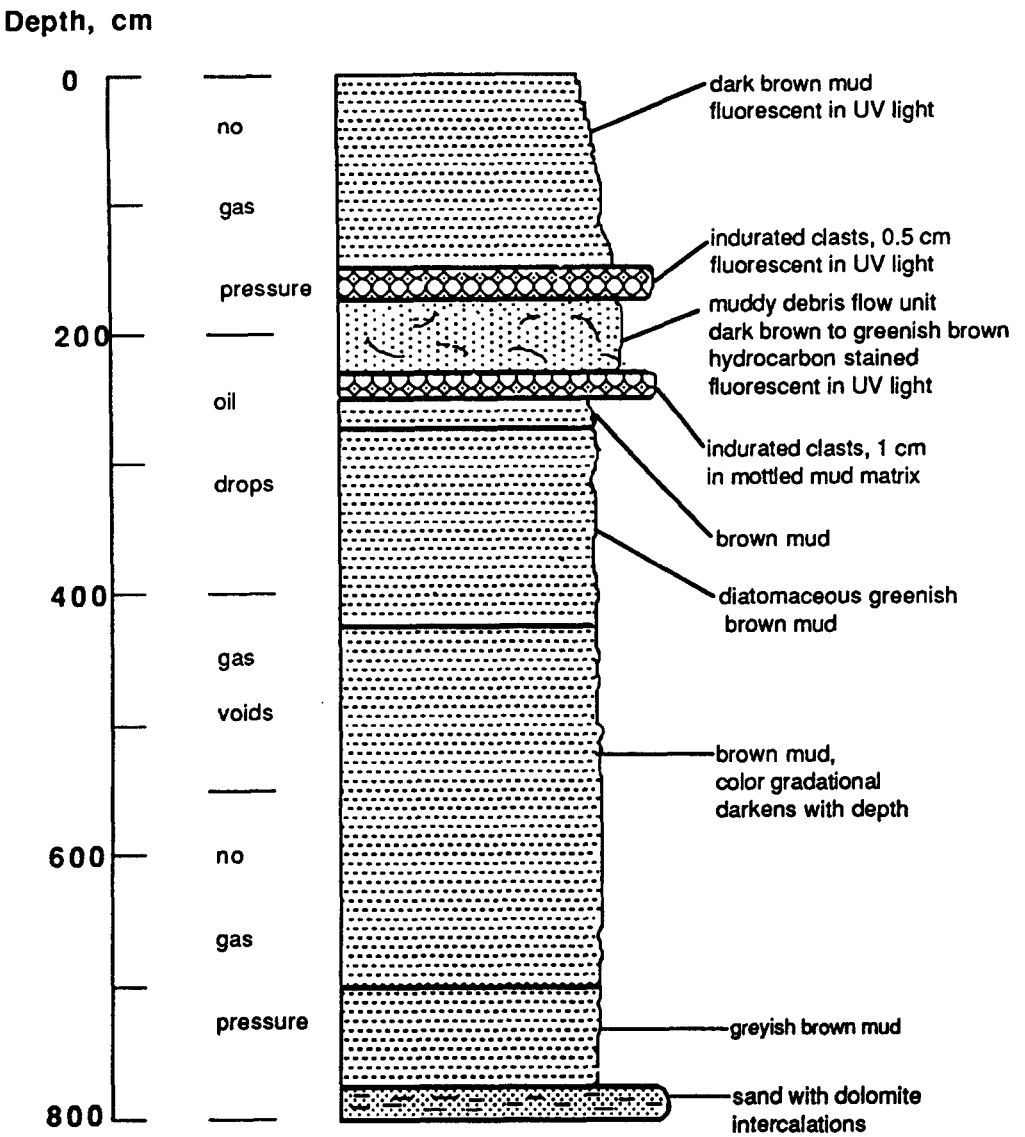

Fig. 2. Lithologic description for core PC6. Note that the depth scale is not known due to loss of the top of the piston core and partly due to potential compaction.

breccia layers, but not in adjacent sediments (Table 2). Barite has been documented as a secondary solid which forms when Ba-laden hydrothermal fluid mixes with sulfate-bearing seawater (Lonsdale *et al.*, 1980; Peter and Scott, 1988; Gieskes *et al.*, 1991; Magenheim, 1989; Magenheim and Gieskes, 1992). The abundance of total calcite (biogenic plus inorganic) generally increases down core. Calcite, however, is absent from the 140–250 cm interval (Table 2). Sturz (1991) suggests that calcite is dissolved under hydrothermal conditions of relatively high effective water/rock ratios (water/rock ratio > 10). Thus, the interval bounded by the breccia layers has an authigenic mineral assemblage that is different from what is observed in adjacent sediments. The interval between 140 and 250 cm depth has been altered to a different extent than adjacent sediments, either prior to deposition as a slump deposit or through unusual fluid flow confined to this interval by the bounding breccia layers.

The interval between 783 cm depth and the base of the core also is mineralogically and texturally different from overlying sediments. Grain size below 783 cm is within the silty sand size range and is coarser than in the overlying units. The relatively coarser grain size within the unit below 783 cm suggests a higher energy environment of transport for this unit than for overlying units, perhaps deposition from a turbidity current.

Mineralogical evidence supporting enhanced fluid flow below 783 cm depth includes the presence of authigenic dolomite, gypsum and heulandite. Dolomite cemented layers of up to 3 mm thickness occur within the silty sand unit, between 789–790, 790–791,

Table 1. Summary of clay mineral relative abundances and relative crystallinities in piston core PC 6 with depth

	Smectite		Illite		Kaolinite	
Depth (cm)	abund.[1]	cryst.[2]	abund.[1]	cryst.[2]	abund.[1]	cryst.[2]
12	96	24	3	2	1	2
46	97	25	3	3		
146	96	21	3	3	1	2
155	98	20	2	2		
164	98	21	2	3		
173	94	22	5	6	1	3
204	100	20				
251	100	19				
267	96	17	3	3	1	3
357	97	15	2	2	1	3
480	95	14	4	2	1	5
561	96	15	1	2	3	3
622	98	17	2	1		
679	98	10	1	3	1	1
698	99	14	1	2		
739	98	11	2	4		
769	97	12	2	3	1	2
784	97	13	2	2	1	2
789	97	10	3	3		
791	97	10	3	2		
795	98	12	3	3		
796	97	11	3	3		
798	98	10	2	2		
core catcher	98	10	2	3		

[1]Clay mineral relative abundances are determined on the less than 2 μm fraction and have been normalized to 100% clays.[2] Clay mineral relative crystallinities are determined by XRD peak width, in mm, at half the maximum height. Tall narrow peaks indicate greater crystallinity than short, broad peaks.

and 794–795 cm depth. Dolomite was visually identified by its rhombohedral morphology and confirmed by XRD analyses. The dolomite layer at 789–790 cm depth is smooth and sharply defined along its lower surface, while the upper surface is irregular, with an undulatory surface. The smoothness and sharp definition of the lower surface suggest that it may be actively plating and dolomite is being added to the lower surface by Mg-bearing fluids circulating below this layer. The dolomite layer at 789–790 cm may be a barrier to upward fluid circulation. The dolomite cemented layers within the 790–791 and 794–795 cm intervals are less regular and more lenticular in shape. Petrographic examination of the 789–790 cm depth interval reveals quartz, feldspar, biotite, and amphibole as detrital grains with corroded boundaries and their presence is confirmed by XRD analyses of the bulk sediment from this interval. Microcrystalline

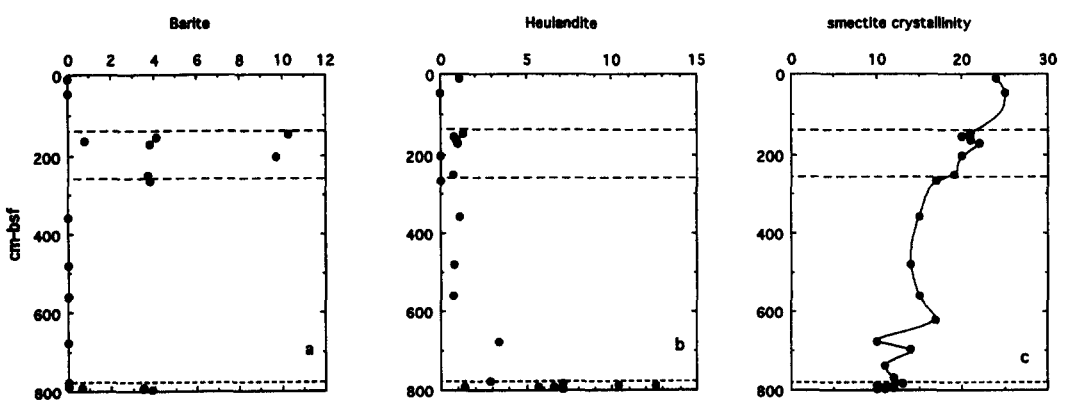

Fig. 3. Mineralogy of core PC6. Data for barite and heulandite are in terms of abundance index, cf., Table 2. data for smectite are in terms of crystallinity index, cf., Table 1. Note that crystallinity index number, peak width at its half maximum height, decreases with greater crystallinity.

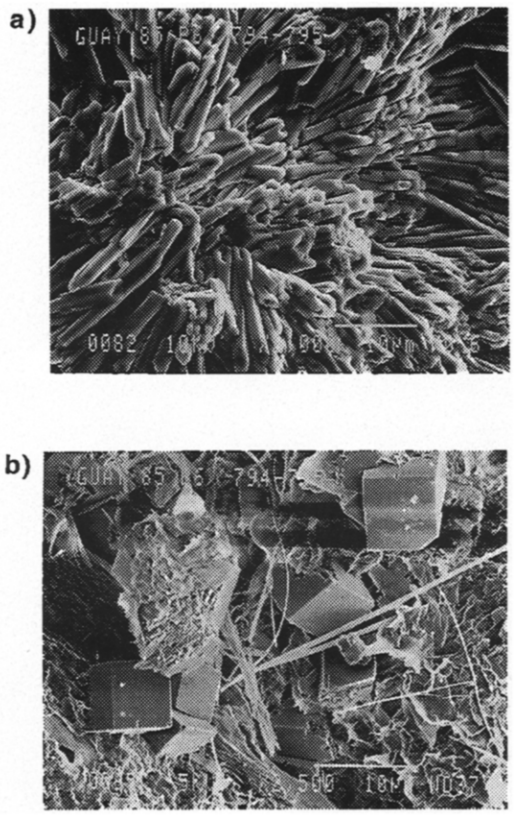

Fig. 4. SEM photographs of the dolomitized layer within the sandy unit, 794–795 cm depth. (a) Resorbed gypsum; (b) well formed dolomite and smectite. Bar is 10 μm.

Table 2. Abundance index of secondary minerals in piston core PC 6 with depth[1]

Depth (cm)	Dolomite	Gypsum	Barite	Heulandite	Calcite
12				1.1	2.4
46					1.8
146			10.3	1.3	
155			4.1	0.8	
164			0.8	0.9	
173			3.8	1.0	
204			9.7		
251			3.7	0.7	
267			3.8		1.4
357				1.1	2.1
480				0.8	3.1
561				0.7	4.4
679				3.4	4.9
779	0.2			2.9	2.2
783	0.3			7.1	
788	8.4			10.4	0.8
789	22.2			12.6	0.7
791	24.5	0.9	0.6	5.7	0.8
792		1.1	3.5	6.6	
793	23.6			1.4	
794	14.4	1.1			
795	12.9	0.9		7.1	0.5
796	0.7	1.0	3.9	7.1	2.6

[1]Abundance index is based on XRD peak area. It is a semiquantitative indication of relative abundance and can only be applied to single minerals at various depths in the core. The abundance index cannot be used to compare abundances of different minerals.

dolomite is present as a coating on many detrital mineral grains, occurs as space filling within foraminifera test chambers, and appears as rhombohedral crystals dispersed throughout the interval below the smooth dolomite layer at 789–790 cm depth. SEM photographs of the 794–795 cm interval show poorly formed, irregular gypsum crystals (Fig. 4a) and rhombohedral dolomite with a clay mineral (Fig. 4b). The poorly formed, irregular crystals of gypsum suggest that gypsum is dissolving. XRD analysis confirms the identification of gypsum in the 794–795 cm depth interval (Table 2).

Heulandite is present in trace amounts with poor crystallinity above 783 cm depth (Table 2). Below 783 cm depth, heulandite increases in relative abundance, and XRD peaks are intense, sharp, and well-formed, indicating an increase in heulandite crystallinity.

Bulk sediment chemical composition

The major element composition of the bulk sediments is presented in Table 3. The data are reported in terms of % oxides, but to investigate the potential changes in composition use is made of the elemental ratio to Ti. Magenheim and Gieskes (1992) argued that the mobility of Ti under hydrothermal conditions would likely be less than that of aluminum. Though this contention may be a subject of future scrutiny, changes in elemental ratios from background values will serve as indicators of alteration of the solid phases. The element to Ti ratios are presented in Fig. 5a and b (the latter figure emphasizing the lowermost part of the core). The debris flow unit between 140 and 250 cm is characterized by relative depletions in the Al/Ti, the Fe/Ti, and the Si/Ti ratios, whereas the ratio of Mg/Ti shows very large increases. This is also evident from the high MgO concentrations reported in Table 3, increasing up to 14% in the 140–250 cm layer. The highest MgO concentrations occur at the top and the bottom of the slump deposit, indicating more substantial alteration. Similarly, the sediments below 782 cm again indicate decreases in the ratios of Al/Ti, Fe/Ti, Si/Ti, with some variability in the ratios of K/Ti and Mg/Ti. The vertical dashed lines in Fig. 5a and b represent "average ratios" for the relatively unaffected sediments, and these ratios agree well with the average background levels established for the hydrothermally unaffected core of the study of Magenheim and Gieskes (1992).

Pore water chemical composition

The pore water chemical composition (Fig. 6) can be used to identify fluid source and to infer chemical reactions between fluids and solids which are active in the sedimentary section at the time of sampling. It is important to note that pore waters indicate recent conditions, whereas the chemistry of the solid phases represents longer term changes in the chemical composition. Pore water concentration–depth profiles for PC 6 are described in detail elsewhere (Gieskes *et al.*, 1988, 1991; Simoneit *et al.*, 1992).

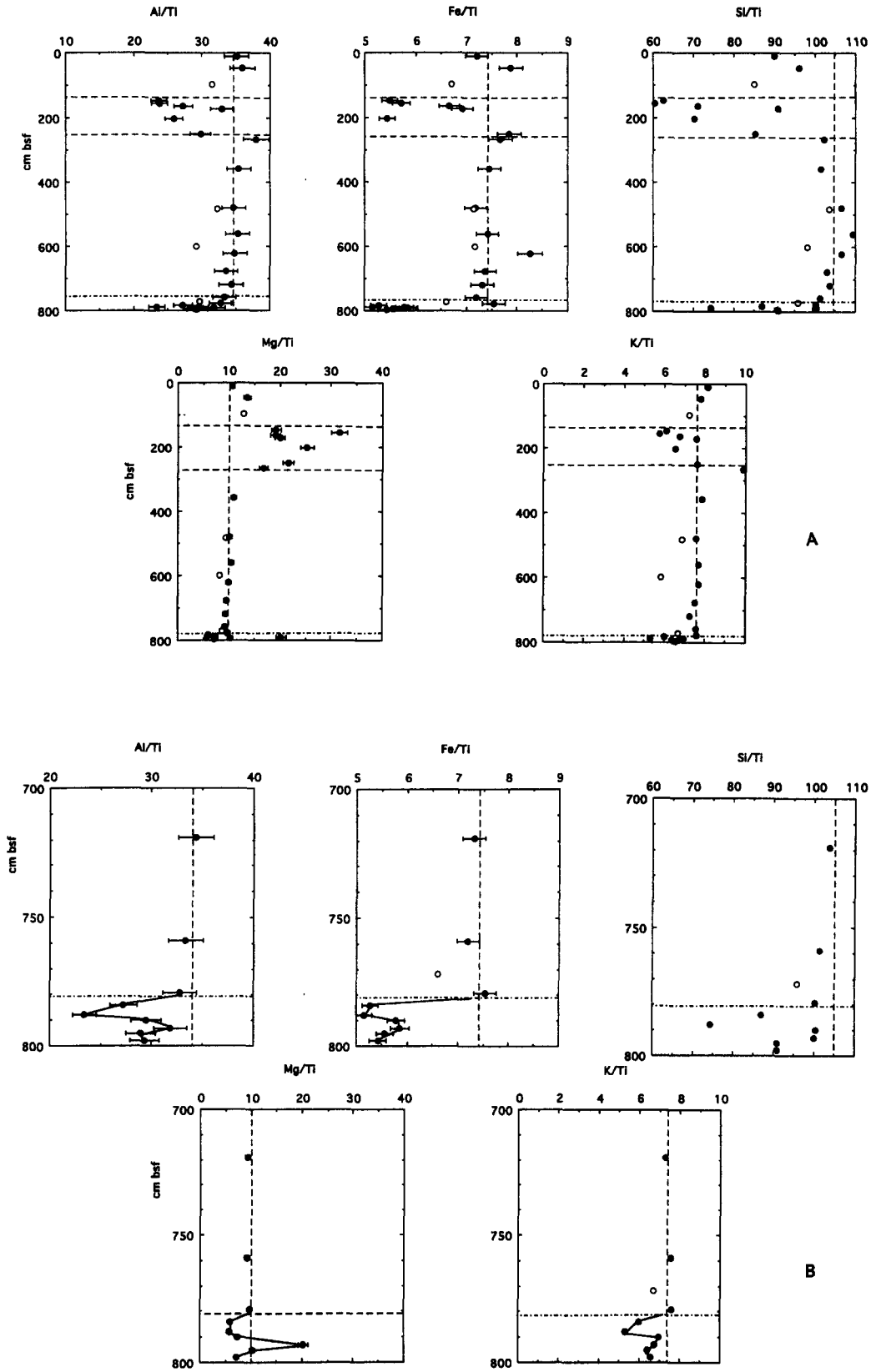

Fig. 5. Element/Ti molar ratios vs depth of bulk sediments of core PC6. (a) Entire core. Note horizontal bars delineate special zones in sediments (see text). (b) Details of lower part of the core. Vertical dashed line represents typical value for a background core in Guaymas Basin (Magenheim and Gieskes, 1992). Connecting lines are intended to guide the eye only.

Table 3. Chemical analysis of sediments of Core PC 6

Depth (cm)	SiO_2 (%)	Al_2O_3 (%)	TiO_2 (%)	Fe_2O_3 (%)	K_2O (%)	CaO (%)	MgO (%)
11	46.45	15.40	0.34	4.94	3.29	1.95	3.69
46	52.78	16.77	0.37	5.75	3.35	2.12	5.03
96*	51.10	16.06	0.40	5.36	3.40	1.29	5.15
146	41.24	13.20	0.44	4.80	3.15	1.60	8.46
155	41.36	13.82	0.45	5.19	3.08	1.75	14.54
163	43.75	14.22	0.41	5.44	3.25	1.99	7.87
173	48.09	14.78	0.35	4.86	3.14	2.02	7.07
203	44.62	13.97	0.42	4.59	3.25	1.60	10.79
250	45.37	13.46	0.35	5.54	3.18	1.98	7.71
267	52.69	16.62	0.34	5.26	3.99	1.97	5.77
357	48.98	14.53	0.32	4.78	2.98	1.98	3.53
480	55.15	15.24	0.34	4.94	3.07	2.16	3.49
482*	55.95	14.84	0.36	5.14	2.92	3.33	3.39
561	54.95	15.04	0.33	4.95	3.03	2.20	3.50
600*	58.95	14.89	0.40	5.71	2.74	3.36	3.26
621	53.50	14.84	0.33	5.51	3.03	2.27	3.32
679	58.65	16.26	0.38	5.58	3.37	2.27	3.64
719	56.25	15.80	0.36	5.27	3.08	2.35	3.40
772*	57.64	15.14	0.40	5.26	3.16	1.99	3.51
759	54.98	15.34	0.36	5.19	3.22	2.28	3.36
779	58.47	16.21	0.39	5.84	3.47	2.26	3.83
784	61.14	16.26	0.47	4.94	3.31	2.20	2.80
788	56.37	15.04	0.50	5.18	3.14	2.40	2.88
790	62.51	15.60	0.41	4.79	3.40	2.44	3.08
793	51.13	13.82	0.34	3.98	2.71	6.44	6.95
795	53.02	14.33	0.39	4.31	2.91	3.31	3.99
798	58.49	16.01	0.43	4.64	3.31	2.54	3.09

Depth (cm)	Fixed NH_4^+/AlC	Exchangeable NH_4^+/Al
96	0.0141	0.0009
208	0.1128	0.0109
299	-	0.0089
316	0.0336	0.0049
482	0.0165	0.0023
598	-	-
600	0.0188	0.0054
698	0.0319	0.0064
772	0.0070	0.0004
779	-	-
799	0.0099	0.0075

*Analyses by X-ray fluorescence spectroscopy.

The following is a brief discussion of these data. The pore water concentration–depth profiles show considerable complexity (Fig. 6) as a result of several processes affecting pore waters in these sediments: (1) A contribution from a hydrothermal component is indicated by elevated levels of dissolved chloride; (2) Increases in dissolved potassium suggest that the chloride enriched fluids below the base of the core are also potassium rich, thus suggesting that the hydrothermal reactions leading to these increases must have exceeded 150°C (Seyfried and Bischoff, 1979); (3) The dolomite layers below ~685 cm act as a boundary to upward flow at this time, only allowing diffusive communication with hydrothermal fluids below, as is evident from the potassium and chloride concentration depth gradients; (4) Increases in dissolved sulfate, calcium, and perhaps strontium suggest dissolution of gypsum-anhydrite below the dolomite layers; (5) Sulfate reduction and secondary calcite formation are indicated in the middle section of the core, with sulfate being supplied from both above and below these depth horizons by diffusive exchange; (6) Dissolved ammonium reaches maximum concentrations at a depth of about 600 cm, well below the minimum in dissolved sulfate at ~450 cm. Uptake of ammonium in clays (e.g., Sterne *et al.*, 1982) (perhaps causing some of the increase in dissolved potassium through ion exchange) at about 800 cm may, in part, explain the sharp decrease in dissolved NH_4^+ below 500 cm (Table 3); (7) Dissolved magnesium is relatively unaffected in the main sulfate reduction zone above 400 cm depth. The decrease of magnesium towards ~700 cm may be related to a combination of processes, including ongoing uptake of Mg in clays and/or dolomite and mixing of pore fluids with a low-Mg fluid.

Pore water chemical concentration gradients in the upper three quarters of the core are smooth, and

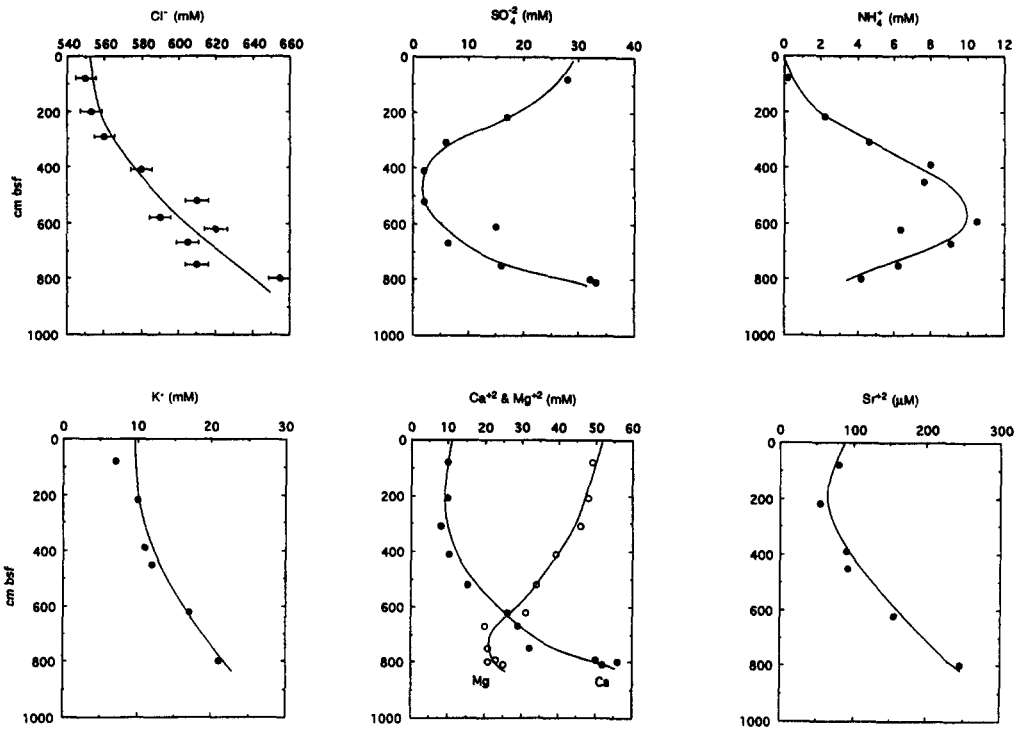

Fig. 6. Pore water chemical gradients in core PC6.

appear to be unaffected by lithological and mineralogical changes down core. The pore water data above 500 cm depth give no indication for the presence of a channel with enhanced fluid flow at this time. Pore water profiles above 500 cm depth are typical for calcium, sulfate, ammonium and magnesium ion concentration gradients for anoxic sediments. These gradients form because sulfate reduction, organic matter degradation, and clay mineral recrystallization are active processes. Slight mimima in calcium and strontium gradients are due to calcium carbonate precipitation reactions.

Evidence for the presence of a hydrothermal fluid component below 800 cm is represented by the large increase in dissolved chloride with depth (Gieskes *et al.*, 1988; Magenheim, 1989), as well as large increases in calcium, strontium, and potassium concentrations. However, the major increases in sulfate, calcium and strontium concentrations towards the base of the core are mainly the result of gypsum dissolution, with the sharp gradients above 800 cm indicating diffusive exchange with the overlying sediments. Dissolution of previously formed secondary solids indicates a change in fluid composition from some previously circulating fluid. That is, pore water data suggest that hydrothermal fluids are presently circulating in sediments near the base of PC 6, probably confined below the dolomite layer. Pore water concentration/depth profiles give no indication of presently active enhanced fluid circulation in the upper unit between 140 and 250 cm depth.

Organic carbon, bitumen composition and volatile hydrocarbons

The organic geochemistry of Core PC 6 has been described in detail elsewhere (Simoneit *et al.*, 1992), but here we present the organic geochemical evidence, which is directly relevant to the description of the transient nature of the effects of hydrothermal interactions on these sediments.

Organic matter character. The organic carbon contents and the information from the Rock–Eval analyses of the organic matter are presented in Table 4 and in Fig. 7. A gradual decrease in organic carbon occurs with depth, but below 775 cm, the decrease in organic carbon sharpens. Rock–Eval can yield an estimate of oil and gas potential (Production Index) by calculation of the relative abundance of free hydrocarbons versus the sum of free hydrocarbons plus hydrocarbons produced by kerogen cracking. In general, the Production Index, PI, will increase with burial depth and maturation during normal burial diagenesis. PI will be relatively large in zones of hydrocarbon maturation. Two PI maxima (Fig. 7b) occur in the hydrocarbon rich sediments between 140 and 250 cm and below 782 cm depth, indicating high maturity, i.e., the wet gas window (Tissot and Welte, 1984), at the bottom of the core. The presence of hydrocarbon stains and the high bitumen extract yield (Simoneit *et al.*, 1992) within the 140–250 cm interval confirm that high molecular weight hydrocarbons are abundant in this interval. Rock–Eval can also

Table 4. Percent organic C and Production Index, H Index and O Index versus depth from piston core PC 6 sediments

Depth	Organic C	Production Index	H Index	O Index
96	2.15	0.13	93	8
208	1.96	0.28	244	24
299	1.61	0.09	102	142
316	1.31	0.15	126	149
482	1.66	0.10	110	116
598	1.67	0.14	69	24
600	1.42	0.09	127	203
698	1.43	0.06	91	91
772	1.20	0.12	69	85
779	0.90	0.22	52	60
799	0.30	0.37	40	282

characterize the type of organic matter present and its thermal evolution. By plotting the Hydrogen Index, HI, against Oxygen Index, OI, on a modified van Krevelen diagram the organic matter in sediments is classified as Type I, II, or III, with Type I being marine and oil prone, Type III being terrestrial and gas prone, and Type II being intermediate. The HI/OI diagram (Fig. 7c) suggests the presence of mostly terrestrial organic carbon, but in this case, involving hydrothermally altered sediments, there is a problem with simple interpretation of the van Krevelen diagram. The relatively high OI values do suggest, however, that conventional oil cannot be generated from the organic matter in the cored section of the sediments and that the kerogen has been thermally altered (Peters *et al.*, 1983; Peters and Simoneit, 1982). The carbonate was not removed from these samples prior to Rock–Eval analysis because in an earlier study it was found that acid leaching removed a significant amount of hydrolyzable organic matter, yet did not significantly alter the OI (Peters and Simoneit, 1982). In addition, the estimated age (^{14}C) of the total organic matter at 8 mbsf in the Southern Trough is ~2000 years B.P. (Spiker and Simoneit, 1982). This is much younger than the organic detritus at such depths in conventional sedimentary basins. Hydrous pyrolysis of this sediment type confirms this inference. The bitumen thus produced is rich in polar/asphaltic and not aliphatic material as expected from typical marine organic matter (Leif *et al.*, 1991). This is interpreted to be due to the immaturity of the organic detritus, which has not undergone sufficient diagenesis to mineralize the polar constituents (e.g., amino acids).

Light hydrocarbons. Data for the volatile hydrocarbons are presented in Table 5 and two examples of typical gas chromatograms for the total headspace hydrocarbons are shown in Fig. 8. Volatile hydrocarbon contents of PC 6 sediments range from methane (C_1) to C_9, consisting of benzene and

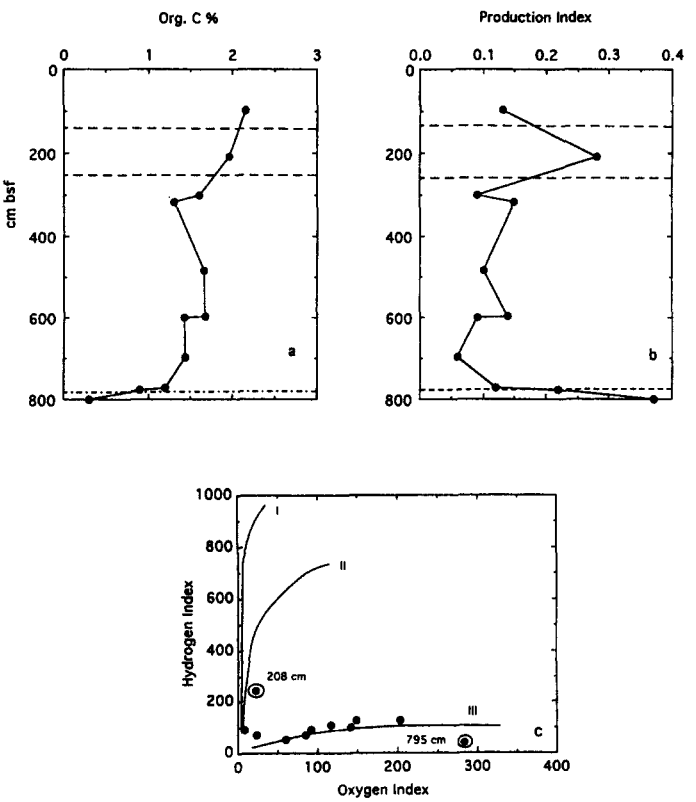

Fig. 7. Organic C contents and Rock–Eval data for core PC6. Circled data points are in "special" hydrothermally affected zones. Connecting lines are intended to guide the eye only.

Table 5. Yields and ratios of volatile hydrocarbons from headspace analyses of piston core PC 6 sediments

Compounds (Concentrations in ppm, v/v)	Subbottom depth (cm)				
	86–91	239–244	392–397	503–508	653–658
methane, C_1	56	3272	3590	5890	1196
ethane, C_2	14	54	113	205	49
propane, C_3	13	11	98	258	80
iso-butane, i-C_4	3	2	42	150	51
n-butane, n-C_4	3	2	45	168	73
iso-pentane, i-C_5	1	0.8	20	95	59
n-pentane, n-C_5	0.8	0.3	10	43	40
cyclopentane, CP	-	0.1	5	14	10
iso-hexane, i-C_6	-	-	1.6	9	17
anteiso-hexane, a-C_6	-	0.8	0.6	4.1	9.4
n-hexane, n-C_6	-	-	1.4	4.1	12
methylcyclopentane, MCP	-	0.3	7.3	18	27
n-heptane, n-C_7	-	-	1.3	1.2	4.7
Ratios					
$C_1/(C_2+C_3)$	2.1	50	17	13	9.3
$C_1/(C_2-C_5)$	1.6	47	11	6.4	3.4
n-C_4/i-C_4	1.3	1.0	1.1	1.1	1.4
n-C_5/i-C_5	0.8	0.3	0.5	0.5	0.7
a-C_7/DMCP[a]	-	-	0.3	-	0.1
n-C_7/Tol[b]	-	-	0.6	0.4	2.0
DMCP Index[c]	-	-	49	38	39

[a] *anteiso*-heptane to dimethylcyclopentanes ratio (Simoneit *et al.*, 1988).[b] *n*-heptane to toluene ratio (Simoneit *et al.*, 1988).[c] Dimethylcyclopentane index (Simoneit *et al.*, 1988).

alkylbenzenes in addition to normal, branched and cyclic alkanes (Simoneit *et al.*, 1992). The volatile hydrocarbon distribution indicates an origin primarily from thermal cracking of heavier organic matter (similar examples are given by Whelan *et al.*, 1988; Gieskes *et al.*, 1988; Simoneit *et al.*, 1988). The highest concentrations of $C_1 - C_4$ hydrocarbons are observed in the 503–508 cm section of the core, which corresponds to the interval with gas voids (i.e., voids due to gas expansion upon core recovery—Fig. 2). This is also in the zone where sulfate approaches zero in concentration (Fig. 9). In part this distribution can be understood by the consumption of the lighter hydrocarbons by sulfate reducing bacteria at greater depths in the core and by loss from diffusion and water washing and/or biodegradation in the shallower

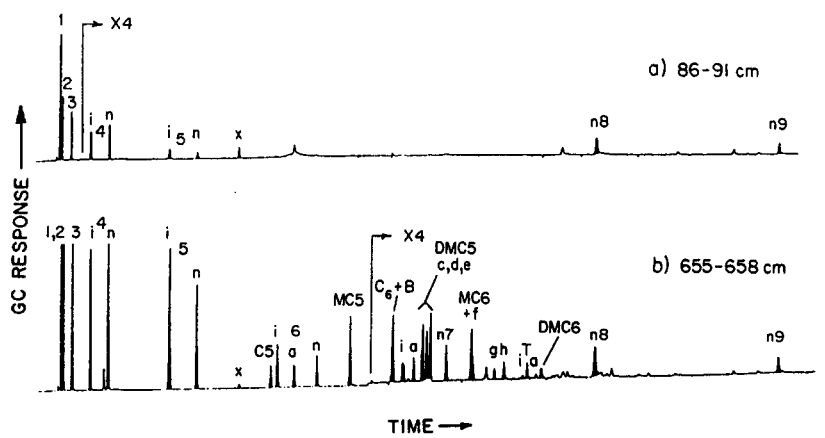

Fig. 8. Examples of gas chromatograms of the volatile hydrocarbons (C_1–C_9) in the headspace of sediment samples from core PC6: (a) 86–91 cm; (b) 653–658 cm. [GC conditions; column 30 m x 0.32 mm i.d. coated with DB-5 (J + W); oven was temperature programmed from −25°C (hold for 1 min) to 150°C at 40°C min^{-1}, then to 300°C at 25°C min^{-1} (hold for 5 min)]. Numbers refer to C chain length with: n = normal, i = *iso*-(2-methyl-) and a = *anteiso*-(3-methyl-) of the corresponding chain length. Cyclic compounds are: c = cyclo-, MC = methylcyclo-, DMC = dimethylcycloalkanes. The DMC5 triplet contains the c = cis-1,3-, d = trans-1,3-; e = trans-1,2-isomers. Others are: f = 1,1,3-trimethylcyclopentane; g = 1,2,4-trimethlcyclopentane; h = 1,2,3-trimethylcyclopentane; B = benzene; t = toluene; x = CH_2Cl_2 contaminant.

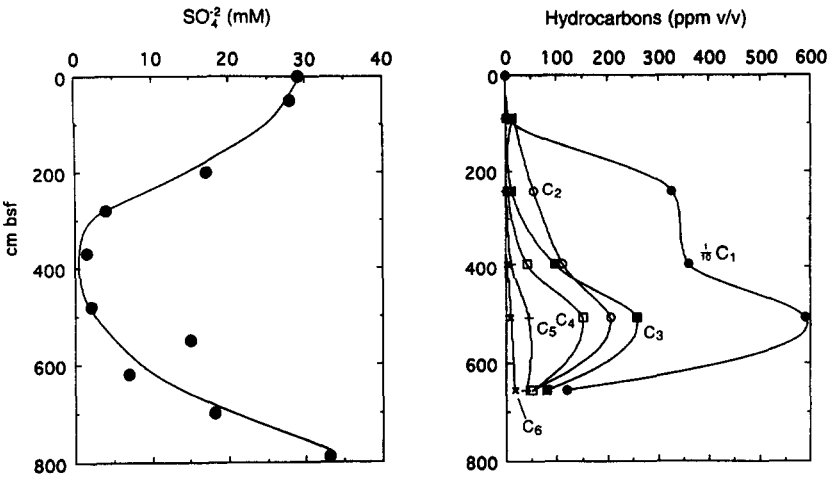

Fig. 9. Distribution of dissolved SO_4 and C_1–C_6 hydrocarbons in core PC6.

section. As a consequence the heavier hydrocarbons ($C_5 - C_9$) become increasingly enriched with depth.

The thermogenic origin of the gases is supported by their $C_1/(C_2+C_3)$ ratio (Table 5) ranging from 2 to 50, which is typical for such a source and consistent with previous studies of samples from Guaymas Basin (Simoneit *et al.*, 1988; Whelan *et al.*, 1988). Various hydrocarbon ratios have been calculated on a weight basis (e.g., per g carbon) to be consistent with previous studies of samples from Guaymas Basin. The pentane ratio ($n\text{-}C_5/i\text{-}C_5$) monitors the thermally-controlled normal to branched character of the hydrocarbons (Whelan *et al.*, 1988). The pentane ratio ranges from 0.3 to 0.8, suggesting a lower thermal stress for volatiles than the majority of the vent water samples and hydrothermal mound oils analyzed previously (0.2–1.1, Simoneit *et al.*, 1988). The ratio of 3-methylhexane (*anteiso*-C_7) to the dimethylcyclopentane (DMCP) triplet is a measure of the paraffinic composition (Thompson, 1979; Simoneit *et al.*, 1988). The relatively low values of 0.3 and 0.1 at 392–397 and 653–657 cm subbottom, respectively, compared to typical values of 0.4–0.7 may indicate biodegradation. The $n\text{-}C_7$/toluene ratio is an indicator of the paraffinic/aromatic character. The range of 0.3–2.0 reflects a significant aromatic character, most likely due to the greater aqueous solubilities of the aromatic compounds transported via the pore fluids. The values of the dimethylcyclopentane (DMCP) Index are grouped close together and range in value from 38 to 49, falling in the same range as samples analyzed previously (Simoneit *et al.*, 1988). This index is a measure of the percent of 1,2-dimethylcyclopentane in the dimethylcyclopentane isomer triplet and is an indicator of biodegradation. The lower concentrations of volatile hydrocarbons at shallower depths (< 2 mbsf) are mainly due to their biodegradation and possible diffusion into the overlying bottom water.

Bitumen composition. The yields for the bitumen extracts are given in Table 6. There is a large amount of extractable petroleum at about 240 cm in the debris flow. Below the debris flow, the amount of extractable organic matter drops and remains relatively constant. The thermal maturity of these bitumens will be assessed in order to differentiate between migrated and *in situ* altered organic matter.

Typical examples of gas chromatograms of some aliphatic fractions separated from the bitumen extract are presented in Fig. 10. The uppermost sample (86–91 cm) has a moderate bitumen yield, a bimodal unresolved complex mixture (UCM), and the homologous *n*-alkane series, ranging from C_{15} to C_{30}, is unique in this sample set in having an uncommon even/odd carbon number predominance. Specific compound distributions and molecular indicators (e.g., biomarkers, PAH, Simoneit *et al.*, 1992) indicate this material is diagenetically advanced, but has not experienced extensive thermal alteration (< 150°C). Although maturation is time and temperature dependent (Philippi, 1965; Connan, 1974; Hunt, 1979), thermal stress in hydrothermal systems occurs over brief time intervals and one can make an upper limit temperature estimate for the rapid organic matter alteration based on laboratory hydrous pyrolysis simulations. The aliphatic fraction of the 239–244 cm depth interval (Fig. 10a), corresponding to the debris flow unit, has a large bitumen yield with a predominant *n*-alkane component in the C_{15}–C_{25} range, and may be indicative of an origin from marine organic matter (Brassell *et al.*, 1978). The smooth distribution is similar to a mature reservoir petroleum (Tissot and Welte, 1984), as is confirmed by specific molecular markers (biomarkers) (Simoneit *et al.*, 1992) and indicates a maximum generation temperature of 200–350°C depending on exposure time. Aliphatic fractions of other subsamples from the debris flow (173–175 cm, 226–228 cm) exhibited similar gas chromatograms.

The aliphatic extracts from the 392–397 cm and 503–508 cm depth intervals (e.g., Fig. 10b) are similar

Table 6. Yields and gross composition of extractable organic matter from piston core PC 6

Depth (cm)	Bitumen yield (mg/g dry sediment)	Saturates (% wt.)	Aromatics (% wt.)	NSO compounds + Asphaltenes (% wt.)
86–91	3.82	7.4	13.3	79.3
173–175	tr.	n.d.	n.d.	n.d.
226–228	tr.	n.d.	n.d.	n.d.
239–244	12.38	21.3	19.8	58.9
392–397	0.76	3.4	6.1	90.5
503–508	0.87	2.7	5.1	92.2
653–658	0.83	2.3	7.1	90.6
798–799	0.94	n.d	n.d.	n.d.

tr. = trace (due to low amount of subsample). n.d. = not determined.

in composition and contrast with the shallower sections. These samples have low bitumen yields and extremely low amounts of *n*-alkanes relative to other components. A significant amount of these constituents are C_{19} and C_{20} olefins, sterenes, and triterpenes. These compounds occur in the early stages of transformation of organic matter from the original source materials to the residual sedimentary organic products, which implies that these sediments are possibly undergoing thermally enhanced diagenesis (e.g., dehydration reactions of lipid compounds with maximum exposure temperatures $<100°C$) as

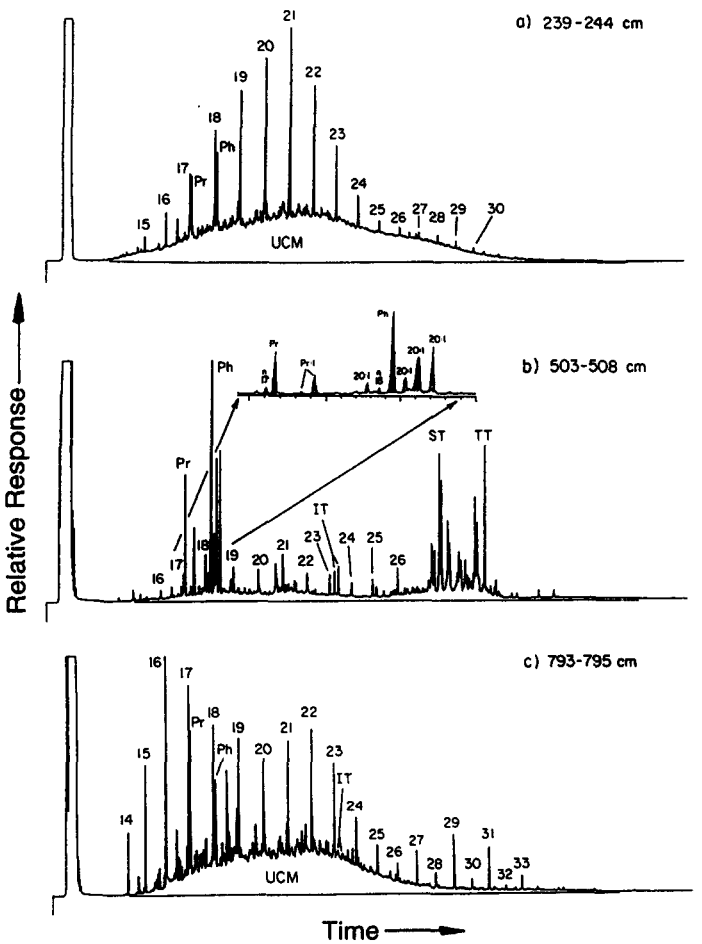

Fig. 10. Examples of gas chromatograms of the hydrocarbon (aliphatic) fractions of the extracted bitumen from the sediments samples of core PC6: (a) 239–244 cm; (b) 503–508 cm; (c) 793–795 cm [GC conditions: column 30 m x 0.32 mm i.d. coated with DB-5 (J&W); oven was temperature programmed from 65°C (hold for 1 min) to 135°C at 25°C min^{-1}, then to 300°C at 4°C min^{-1} (hold for 30 min)]. Numbers refer to C chain length of the *n*-alkanes ip = isoprenoid, Pr = pristane, Ph = phytane, n:1 = C_{19} and C_{20} olefins, ST = steranes, TT = triterpanes, IT = isoprenoid thiophenes, UCM = unresolved complex mixure of branched and cyclic hydrocarbons.

described for Bransfield Strait (Brault and Simoneit, 1988). The presence of major amounts of sterenes and triterpenes implies a minimal amount of thermal alteration of the organic matter.

The aliphatic fraction of the 653–658 cm section, which also has a low bitumen yield, has an immature hydrocarbon distribution similar to those of the 392–397 cm and 503–508 cm sections. The 793–795 cm section (Fig. 10c) is derived from the sandy layer. It has a low bitumen yield and the *n*-alkane distribution ranges from C_{16} to C_{29}, with a strong odd/even carbon number predominance $> C_{23}$. This is characteristic of a significant terrestrial component in the total bitumen (e.g., Brassell *et al.*, 1978; Simoneit, 1978). The biomarker indices show a larger degree of thermal maturity (higher heat flow, maximum generation temperature $< 150°C$) than those of the intermediate depth ranges, but still not as mature as those of the upper samples.

Aromatic hydrocarbons are present in all sections of this core. High molecular weight polycyclic aromatic hydrocarbons (PAH) are concentrated in the shallow intervals (86–71, 173–178, 226–228, and 239–244 cm), that is, the debris flow unit with associated indurated mud and above (Simoneit *et al.*, 1992). These heavy PAH consist of the same suite of compounds as found in the hydrothermal petroleums at the seabed (Kawka and Simoneit, 1990). Low molecular weight PAH (e.g., naphthalenes, phenanthrenes, Diels" hydrocarbon) are also distributed throughout the core and some concentration maxima versus depth occur, especially in the oil zone (173–250 cm interval, Simoneit *et al.*, 1992). The redistribution of low molecular weight PAH by fluids was tested with various ratios of alkyl PAH to PAH for hydrous pyrolysis experiments of Guaymas Basin mud (Leif, 1993) and comparison with samples from the natural system. Thus the methylphenanthrene indices (e.g., MP/P; MPI_3, Garrigues *et al.*, 1988) do not show any significant depth trends due to greater redistribution of phenanthrene (P) than the alkylphenanthrenes (i.e., MP) by diffusion and solution transport. Then an attempt was made to assess their generation temperatures. The generation temperatures for PAH in laboratory hydrous pyrolysis experiments should be valid for extrapolation to the natural system because hydrothermal petroleum generation is geologically instantaneous (Simoneit and Kvenvolden, 1994). The data yielded no meaningful temperatures which fit with the thermal maturity windows of the biomarkers. This confirms that the P, MP, and other PAH redistributed upward to differing degrees, but with concentrations that dramatically changed from their original distributions.

DISCUSSION

Both the inorganic and the organic geochemistry of Core PC 6 confirm the ephemeral nature of the hydrothermal system active in the Guaymas Basin. Much of the alteration of the sediments is caused by a flow-through of high temperature fluids, which mix with less affected pore fluids or water from the basin bottom (Stout and Campbell, 1983; Magenheim and Gieskes, 1992; Gieskes *et al.*, 1988) causing the precipitation of a variety of minerals. In turn the sediment may become clogged preventing continued flow of fluid, thus leading to potential reversals of reactions that involved hydrothermal precipitation of minerals (e.g., calcium sulfates). Here we summarize this information.

Mineralogical and chemical evidence indicates that the sediments between 140 and 250 cm and below 782 cm have undergone substantial alteration. In the upper altered layer (140–250 cm) barite is an important component, but authigenic clays also characterize this section, probably reflecting the large enrichment in MgO and the corresponding increase in the Mg/Ti ratio. The implication of these observations is that fluid flow consisting of a mixture of hydrothermal fluid (source of barium) with sea water (source of sulfate and magnesium) must have occurred through this section. It cannot be concluded that this fluid flow occurred *in situ* or whether the sediments were redeposited from a nearby hydrothermally altered area as a debris flow. However, there is little doubt that substantial interaction with these fluids flowing through the sediments must have occurred to lead to the large depletions in the Al/Ti, Fe/Ti, and Si/Ti ratios, as well as the substantially increased Mg/Ti ratio.

The organic geochemical evidence indicates the presence of mature oil in this layer, confirming fluid flow or bulk migration through this sediment. A significant amount of hydrothermally generated petroleum has accompanied the hydrothermal fluid flow and invaded the 137–250 cm silty clay unit. This petroleum is not biodegraded, which suggests currently active petroleum migration despite the lack of evidence from the dissolved inorganic constituents in the pore water for concurrent hydrothermal fluid flow. The presence of abundant hydrothermal petroleum within the 137–250 cm interval, more abundant than in the adjacent sediments, is further evidence for past chanelized flow, although this oil migration/invasion appears still to be occurring now. Petroleum migration accompanying hydrothermal fluid flow is well documented in Guaymas Basin sediments (Kawka and Simoneit, 1987, 1994; Peter *et al.*, 1990; Simoneit, 1985; Simoneit *et al.*, 1990). This influx of petroleum is confirmed by the PAH. The heavy PAH consist of the same suite of compounds reported for the hydrothermal oils from the seabed (Kawka and Simoneit, 1990) and they were generated at high temperatures of $> 300°C$ prior to redistibution. The sediment cover over this section is at least 140 cm thick, providing a good barrier (seal), considering the fact that piston coring generally loses a substantial part of the surficial sediment. The extracts below the debris flow are thermally immature and that from the sandy layer

below 782 cm has the higher maturity. This indicates that only accelerated diagenesis of the indigenous organic matter (Brault and Simoneit, 1988) has occurred due to the high heat flow.

The volatile hydrocarbon distribution in PC 6 has resulted from the pyrolysis of organic matter at depth (10–30 mbsf) with vertical transport through the cored section resulting in the observed concentration gradients with depth (Fig. 9). However, there is an enrichment of C_1–C_4 hydrocarbons in the 400–550 cm section of the core, where high *in situ* gas pressures developed voids upon decompression during retrieval of the core. The lower amounts of C_1–C_4 hydrocarbons below this interval, with the concomitant increase in C_6, are interpreted to be the result of the migration of supercritical CH_4–C_4H_{10} fluid phase (Didyk and Simoneit, 1990; Simoneit *et al.*, 1988) upward into a lower temperature zone. This leaves behind a C_1–C_4 hydrocarbon depleted mixture at greater depths. More rapid migration/transport of C_1–C_3 hydrocarbons than the C_4 and higher hydrocarbons away from intrusive heat sources was described for DSDP Site 481 in the Guaymas Basin (Curray *et al.*, 1982a). This migration/transport is different and distinguishable from the geochromatography of C_1–C_5 hydrocarbons upward in the laminated sediments of DSDP Hole 479 (Curray *et al.*, 1982b). The naphthenic character (high content of branched and cyclic compounds) of the volatiles could be due to microbial degradation as supported partly by the a-C_7/DMCP ratio and the DMCP Index (Table 5) (Simoneit *et al.*, 1988). The significant aromatic character of the volatiles, as determined by the *n*-C_7/toluene ratio, is most likely attributable to an influx of the more water soluble, volatile aromatics by pore water transport.

Lower molecular weight PAH are distributed throughout the core and their broader distribution is due to the greater solubility of these PAH in water with their subsequent redistribution by pore water transport (Kawka and Simoneit, 1990, 1994; Simoneit *et al.*, 1992). The high enrichment of phenanthrene relative to the alkylphenanthrenes also supports the greater water solubility of the former compound with the subsequent enrichment up the core as a result of fluid migration. This aqueous redistribution of PAH is less pronounced compared to the short core (1630-AC), taken next to an actively advecting vent system, where primarily water soluble, volatile PAH and alkyl PAH were detected (Gieskes *et al.*, 1988). Due to the redistribution of the phenanthrene series, the maturity indices (e.g., MP/P, MPI) could not be applied to the samples from core PC6 and the phenanthrenes could also not be used as thermal probes. The examination of the alkyl–aromatic to parent aromatic ratios did not yield meaningful temperature correlations which fit with the biomarker maturity indices. This confirms that phenanthrene/anthracene, being more water soluble than their alkyl homologs, are redistributed up the core by fluid migration, whereas less soluble biomarkers are retained in the organic phases. In general these ratios for the PAH indicated generation temperatures of <200°C in the zones without the oil and 350–400°C for the sample in the oil zone. However, this is not a well constrained result and only applies to the PAH of the oils.

Below 782 cm chemical changes in the sediments again have led to depletions in the Al/Ti, Fe/Ti, and Si/Ti ratios, but barite is less common. On the other hand, the occurrence of both gypsum and dolomite (the latter with temperatures of formation between 65 and 72°C) require the presence of both magnesium and sulfate. Thus, the fluids causing the hydrothermal alteration of the sediments must have constituted mixtures of pore fluids containing magnesium and sulfate with hydrothermal fluids without sulfate and magnesium, as is typical for high temperature fluids emanating from vents in Guaymas Basin (e.g., Gieskes *et al.*, 1988).

Interstitial water samples show evidence for an input of hydrothermal fluids which appear to be present below the bottom of the core, typically leading to increased concentrations in chloride and potassium (cf., Gieskes *et al.*, 1988). On the other hand, temperatures must have been higher in the past when gypsum was forming. Presently active cooler fluids result in redissolution of gypsum at depths below 782 cm. This phenomenon is reflected in the increase in dissolved sulfate with depth below a broad minimum at about 400 cm and is apparent in the gypsum crystal morphology (Fig. 4a). This may also be the cause of the observed maxima in the lighter hydrocarbons (C_1–C_5), which at present may undergo degradation as a result of bacterial sulfate reduction. The lighter hydrocarbons must have been emplaced during the period of more intense hydrothermal activity which affected these sediments in the past. The concentration depth gradients of the pore water constituents do not suggest that presently pore fluid flow occurs in these sediments. In fact communication with a potential reservoir of hydrothermal fluid below the bottom of the core appears to be diffusive in nature.

SUMMARY AND CONCLUSIONS

In summary, based on texture, mineralogy, and pore water and bulk sediment chemical compositions, we suggest that: (1) the interval between 140 and 250 cm has been altered by hydrothermal fluid flow to a greater extent than sediments above and below; (2) fluid flow in the 140–250 cm interval is no longer active; and (3) the interval between 783 cm and the bottom of the core is presently being altered to a greater extent than the sediments above, with retrograde dissolution of gypsum leading to large increases in dissolved sulfate, calcium, and strontium towards the bottom of the core.

The organic matter distribution also reflects these differences (Simoneit *et al.*, 1992). Hydrothermal

petroleum migrated into the debris flow unit, especially into the 239–244 cm interval, as bulk phase after the major fluid flow ceased. Subsequently the more water soluble compounds such as lower molecular weight PAH were redistributed upward to the seabed. The deeper intervals, specifically from 400 to 550 cm subbottom, have experienced accelerated diagenesis due to high heat flow. This diagenesis increases progressively to the bottom of the core.

Of fundamental importance to investigations of dispersed fluid flow in Guaymas Basin sediments is the overall, basin wide significance of dispersed fluid flow. The question arises as to the quantitative significance of this type of fluid flow. Fisher and Becker (1991) suggest that the influence of dispersed fluid flow, although not trivial, is only a relatively small contributor to the overall heat budget of this hydrothermal system. However, the question remains as to the significance of dispersed fluid flow to the geochemical budget of the deeper waters below the sill, which separates Guaymas Basin from the adjacent Carmen Basin (Campbell and Gieskes, 1984).

Hydrothermal alteration of sediments in the Southern Trough of the basin is well documented. The chemical composition of fluids emanating directly from spires and chimneys has been shown to be constant on a decadal time scale (Campbell *et al.*, 1988). Mineralogical and isotopic studies have shown that the shallow sill intrusions observed at DSDP Site 477 cannot be the source of the high temperature fluids exiting from chimney sites (Kastner, 1982; Gieskes *et al.*, 1982b). That is, the heat and fluid sources are different for the two distinct hydrothermal systems. Campbell and Gieskes (1984) suggest that the observed chemical anomalies in the water column are due to hydrothermal activity and have persisted for at least 20 years. It is unclear what proportion of the chemical anomalies observed in the overlying water column can be attributed to direct fluid flow or dispersed fluid flow. On a volume for volume basis, direct fluid flow will probably have a larger influence on the chemical composition of the overlying water column.

The present study indicates that diffuse fluid flow across the sediment/seawater interface is more variable than direct fluid flow. The observations on surficial sediments (Magenheim and Gieskes, 1992) also indicated that fluid flow directly from the sediments is probably a relatively short term phenomenon, although it leaves a permanent influence in the inorganic and organic chemical composition in the sediments. The data for core PC 6 support this idea.

Acknowledgements—support from the National Science Foundation, Division of Ocean Sciences (Grants OCE-8601316 and OCE-9002366 to BRTS, OCE-8620412 to AAS, and OCE-8631517 to JMG) and from the Chevron Petroleum Technology Company is gratefully acknowledged. We thank Dr. A. P. Gize and Dr. J. Connan for their reviews and comments, which improved the manuscript.

Editorial handling: Dr Ron Fuge

REFERENCES

Brassell S. C., Eglinton G., Maxwell J. R. and Philp R. P. (1978) Natural background of alkanes in the aquatic environment. In *Aquatic Pollutants: Transformation and Biological Effects* (eds O. Hutzinger, T. H. van Lelyveld and, B. C. J. Zoeteman), pp. 69–86. Pergamon Press, New York.

Brault M. and Simoneit B. R. T. (1988) Steroid and triterpenoid distributions in Bransfield Strait sediments: Hydrothermally enhanced diagenetic transformations. In *Advances in Organic Geochemistry, 1987* (eds L. Mattavelli and L. Novelli). *Org. Geochem.* **13**, 697–705.

Brown T. (1988) Wet chemical analysis of marine sediments: Applications to hydrothermal sediments of Guaymas Basin. Master's Thesis, San Diego State University.

Campbell A. C. and Gieskes J. M. (1984) Water column anomalies associated with hydrothermal activity in the Guaymas Basin Gulf of California. *Earth Planet. Sci. Lett.* **68**, 57–72.

Campbell A. C., Bowers T. S., Measures C. I., Falkner K. K., Khadem M. and Edmond J. M. (1988) A time series of vent fluid composition from 21°N, East Pacific Rise (1979, 1981, 1985) and the Guaymas Basin, Gulf of California (1982, 1985). *J. Geophys. Res.* **93**, 4537–4549.

Chan L.-H., Gieskes J. M., You C-F. and Edmond J. M. (1994) Lithium isotope geochemistry of the sediments and hydrothermal fluids of Guaymas Basin, Gulf of California. *Geochim. Cosmochim. Acta* **58**, 4443–4454.

Connan J. (1974) Time–temperature relation in oil genesis. *Amer. Assoc. Petrol. Geol. Bull.* **58**, 2516–2521.

Curray J. R. *et al.* (1982a) Guaymas Basin: Sites 477, 478 and 481. *Initial Reports of the Deep Sea Drilling Project, Leg 64*, Part I, 211-287.

Curray J. R. *et al.* (1982b) Guaymas Basin Slope: Sites 479 and 480. *Initial Reports of the Deep Sea Drilling Project, Leg 64*, Part I, 417-447.

Didyk B. M. and Simoneit B. R. T. (1989) Hydrothermal oil of Guaymas Basin and implications for petroleum formation mechanisms. *Nature* **342**, 65–69.

Didyk B. M. and Simoneit B. R. T. (1990) Petroleum characteristics of the oil in Guaymas Basin hydrothermal chimney. In *Organic Matter Alteration in Hydrothermal Systems – Petroleum Generation, Migration and Biogeochemistry* (ed. B. R. T. Simoneit). *Appl. Geochem.* **5**, 29–40.

Donnelly T. W. (1980) Chemical composition of deep sea sediments — Sites 9 through 425, Leg 2-54, DSDP. *Initial Reports of the Deep Sea Drilling Project* **54**, 899–949.

Eberl D., Whitney G. and Khoury H. (1978) Hydrothermal reactivity of smectite. *Amer. Mineralogist* **63**, 401–409.

Einsele G. (1982) Mechanisms of sill intrusion into soft sediment and expulsion of pore water. *Initial Reports of the Deep Sea Drilling Project, Leg 64*, Part II, 1169–1176.

Einsele G., Gieskes J., Curray J., Moore D., Aguayo E., Aubry M.-P., Fornari D., Guerrero J., Kastner M., Kelts K., Lyle M., Matoba M., Molina-Cruz A., Niemitz J., Rueda J., Saunders A., Schrader H., Simoneit B. and Vacquier V. (1980) Intrusion of basaltic sills into highly porous sediments and resulting hydrothermal activity. *Nature* **283**, 441–445.

Epstein S., Buchsbaum R., Lowenstam H. A. and Urey H. (1953) Revised carbonate-water isotopic temperature scale. *Geol. Soc. Amer. Bull.* **64**, 1315–1326.

Espitalié M., Madec M., Tissot B., Mennig J. J. and Leplat P. (1977) Source rock characterization method for petroleum exploration. *Off Shore Technology Conference, OTC paper* **2935**, 439–444.

Espitalié M., Deroo G. and Marquis F. (1986) La pyrolyse Rock-Eval et ses applications. *Rev. l'Inst. Francais Petrole.* **41**, 73–89.

Fisher A. T. and Becker K. (1991) Heat flow, hydrothermal

circulation, and basalt intrusions in the Guaymas Basin. *Gulf of California. Earth Planet. Sci. Lett.* **103**, 84–99.

Garrigues P., DeSury R., Angelin M. L., Belloq J., Oudin J. L. and Ewald M. (1988) Relation of the methylated hydrocarbon distribution pattern to the maturity of organic matter in ancient sediments from the Mahakam Delta. *Geochim. Cosmochim. Acta* **52**, 375–384.

Gieskes J. M., Elderfield H., Lawrence J. R., Johnson J., Meyers B. and Campbell A. (1982a) Geochemistry of interstitial waters and sediments, Leg 64, Gulf of California. *Initial Reports of the Deep Sea Drilling Project, Leg 64*, Part II, 675–694.

Gieskes J. M., Kastner M., Einsele G., Kelts K. and Niemitz J. (1982b) Hydrothermal activity in the Guaymas Basin, Gulf of California: A systhesis. *Initial Reports of the Deep Sea Drilling Project, Leg 64*, Part II, 1159–1168.

Gieskes J. M., Simoneit B. R. T., Brown T., Shaw T., Wang Y.-C. and Magenheim A. (1988) Hydrothermal fluids and petroleum in surface sediments of Guaymas Basin, Gulf of California: A case study. *Canadian Mineralogist* **26**, 589–602.

Gieskes J. M., Shaw T., Brown T., Sturz A. and Campbell A. (1991) Interstitial water and hydrothermal water chemistry, Guaymas Basin, Gulf of California. In *The Gulf and Peninsular Province of the Californias* (eds J. P. Dauphin and B. R. T. Simoneit). Amer. Assoc. Petrol. Geol. Memoir 47, pp. 753–779.

Hower J., Eslinger E. V., Hower M. E. and Perry E. A. (1976) Mechanism of burial metamorphism of argillaceous sediments, 1. Mineralogical and chemical evidence. *Geol. Soc. Am. Bull.* **87**, 725–737.

Hunt J. M. (1979) *Petroleum Geochemistry and Geology*. W. H. Freeman and Company, San Francisco.

Kastner M. (1982) Evidence for two distinct hydrothermal systems in the Guaymas Basin. *Initial Reports of the Deep Sea Drilling Project, Leg 64*, Part II, 1143–1157.

Kastner M. and Siever R. (1983) Siliceous sediments of the Guaymas Basin: The effect of high temperature gradients on diagenesis. *J. Geol.* **91**, 629–641.

Kawka O. E. and Simoneit B. R. T. (1987) Survey of hydrothermally-generated petroleums from the Guaymas Basin spreading center. *Org. Geochem.* **11**, 311–328.

Kawka O. E. and Simoneit B. R. T. (1990) Polycyclic aromatic hydrocarbons in hydrothermal petroleums from the Guaymas Basin spreading center. In *Organic Matter in Hydrothermal Systems – Petroleum Generation, Migration, and Biogeochemistry* (ed. B. R. T. Simoneit). *Appl. Geochem.***5**, 17–27.

Kawka O. E. and Simoneit B. R. T. (1994) Hydrothermal pyrolysis of organic matter in Guaymas Basin: I. Comparison of hydrocarbon distributions in subsurface sediments and seabed petroleums. *Org. Geochem.* **22**, 947–978.

Kelts K. (1982) Petrology of hydrothermally meytamorphosed sediments at DSDP Site 477, Southern Guaymas Basin Rift, Gulf of California. *Initial Reports of the Deep Sea Drilling Project, Leg 64*, Part II, 1123–1136.

Kelts K. and McKenzie J. (1984) A comparison of anoxic dolomite from deep sea sediments: Quaternary Gulf of California and Messinian Tripoli Formation of Sicily. In *Dolomites of the Monterey Formation and Other Organic-rich Units* (eds L. Garrison, M. Kastner and X. Zinger). *Pacific Section, Soc. Econ. Paleontol. Minerol.*, **41**, 19–28.

Leif R. N. (1993) Laboratory simulated hydrothermal alteration of sedimentary organic matter from Guaymas Basin, Gulf of California. Ph. D. Thesis, Oregon State University, Corvallis, OR.

Leif R. N., Simoneit B. R. T. and Kvenvolden K. A. (1991) Simulation of hydrothermal petroleum generation by laboratory hydrous pyrolysis. In *Organic Geochemistry, Advances and Applications in the Natural Environment* (ed. D. A. C. Manning), pp. 300–303. Manchester University Press, Manchester.

Lonsdale P. and Becker K. (1985) Hydrothermal plumes, hot springs and conductive heat flow in the Southern Trough of Guaymas Basin. *Earth Planet. Sci. Lett.* **73**, 211–225.

Lonsdale P. F., Bischoff J. L., Burns V. M., Kastner M. and Sweeney R. E. (1980) A high temperature deposit on the seabed of the Gulf of California spreading center. *Earth Planet. Sci. Lett.* **49**, 8–20.

Magenheim A. J. (1989) Hydrothermal alteration in near surface sediments of the Guaymas Basin, Gulf of California and the Escanaba Trough, Gorda Ridge. Master's Thesis, University of California, San Diego, pp 146.

Magenheim A. J. and Gieskes J. M. (1992) Hydrothermal discharge and alteration in near-surface sediments form the Guaymas Basin Gulf of California. *Geochim. Cosmochim. Acta* **56**, 2329–2338.

McCrea J. M. (1950) On the isotopic chemistry of carbonates and a paleotemperature scale. *J. Chem. Phys.* **18**, 849–857.

Peter J. M. and Scott S. D. (1988) Mineralogy, composition and fluid-inclusion microthermometry of sea floor hydrothermal deposits in the Southern Trough of Guaymas Basin Gulf of California. *Canadian Mineralogist* **26**, 567–587.

Peter J. M., Simoneit B. R. T., Kawka O. and Scott S. D. (1990) Liquid hydrocarbon-bearing inclusions in modern hydrothermal chimneys and mounds from the soutern trough of Guaymas Basin, Gulf of California. In *Organic Matter in Hydrothermal Systems –Petroleum Generation, Migration, and Biogeochemistry* (ed. B. R. T. Simoneit). *Appl. Geochem.* **5**, 51–63.

Peters K. E. and Simoneit B. R. T. (1982) Rock-Eval pyrolysis of Quaternary sediments from Leg 64, Sites 479 and 480, Gulf of California. *Initial Reports of the Deep Sea Drilling Project* **64**, 925–931.

Peters K. E., Whelan J. K., Hunt J. M. and Tarafa M. E. (1983) Programmed pyrolysis of organic matter from thermally altered Cretaceous black shales. *Amer. Assoc. Petrol. Geol. Bull.* **67**, 2137–2146.

Philippi G. T. (1965) On the depth, time, and mechanism of petroleum generation. *Geochim. Cosmochim. Acta* **29**, 1021–1049.

Seyfried W. E. and Bischoff J. L. (1979) Low temperatutre basalt alteration by sea water: an experimental study at 70°C and 150°C. *Geochim. Cosmochim. Acta* **43**, 1937–1947.

Simoneit B. R. T. (1978) The organic chemistry of marine sediments. In *Chemical Oceanography*, 2nd Edition (eds J. P. Riley and R. Chester), pp. 233–311. Academic Press, New York.

Simoneit B. R. T. (1983a) Organic matter maturation and petroleum genesis: Geothermal versus hydrothermal. In Proc. Symp., *The Role of Heat in the Development of Energy and Mineral Resources in the Northern Basin and Range Province*, pp. 215–241. Geothermal Research Council Special Report No. 13, Davis, California.

Simoneit B. R. T. (1983b) Effects of hydrothermal activity on sedimentary organic matter: Guaymas Basin, Gulf of California – petroleum genesis and protokerogen degradation. In NATO-ARI: *Hydrothermal Processes at Seafloor Spreading Centers* (eds P. A. Rona, K. Bostrom, L. Laubier and, K. L. Smith), pp. 451–471. Plenum Press, New York.

Simoneit B. R. T. (1984) Hydrothermal effects on organic matter—high versus low temperature components. In *Advances in Organic Geochemistry 1983* (eds P. A. Schenck, J. W. de Leeuw and G. W. M. Lijmbach). Pergamon Press, Oxford. *Org. Geochem.***6**, 875–864.

Simoneit B. R. T. (1985) Hydrothermal petroleum: genesis, migration, and deposition in Guaymas Basin Gulf of California. *Canadian J. Earth Sci.* **22**, 1919–1929.

Simoneit B. R. T. and Lonsdale P. F. (1982) Hydrothermal

petroleum in mineralized mounds at the seabed of Guaymas Basin. *Nature* **295**, 198–202.

Simoneit B. R. T. and Kvenvolden K. A. (1994) Comparison of ^{14}C ages of hydrothermal petroleums. *Org. Geochem.* **21**, 525–529.

Simoneit B. R. T., Philp R. P., Jenden P. D. and Galimov E. M. (1984) Organic geochemistry of Deep Sea Drilling Project sediments from the Gulf of California—hydrothermal effects on unconsolidated diatom ooze. *Org. Geochem.* **7**, 173–205.

Simoneit B. R. T., Kawka O. E. and Brault M. (1988) Origin of gases and condensates in the Guaymas Basin hydrothermal system (Gulf of California). In *Proc. Symp. Origins of Methane in the Earth* (ed M. Schoell). *Chemical Geology* **71**, 169–182.

Simoneit B. R. T., Lonsdale P. F., Edmond J. M. and Shanks W. C. III (1990) Deep-water hydrocarbon seeps in Guaymas Basin, Gulf of California. In *Organic Matter in Hydrothermal Systems—Petroleum Generation, Migration, and Biogeochemistry* (ed B. R. T Simoneit). *Appl. Geochem.* **5**, 41–49.

Simoneit B. R. T., Leif R. N., Sturz A. A., Sturdivant A. E. and Gieskes J. M. (1992) Geochemistry of shallow sediments in Guaymas Basin, Gulf of California: hydrothermal gas and oil migration and effects of mineralogy. *Org. Geochem.* **18**, 765–784.

Spiker E. C. and Simoneit B. R. T. (1982) Radiocarbon dating of recent sediments from Leg 64, Gulf of California. *Initial Reports of the Deep Sea Drilling Project* **64**(2), 757–758.

Sterne E. J., Reynolds R. C. and Zantos H. (1982) Natural ammonium illites from black shales hosting a stratiform base metal deposit, Delong Mountains Northern Alaska. *Clays and Clay Mineral.* **30**, 161–166.

Stout P. M. and Campbell A. C. (1983) Hydrothermal alteration of near surface sediments, Guaymas Basin, Gulf of California. In *Cenozoic Marine Sedimentation, Pacific Margin, U.S. A.* (eds D. K. Larue and R. J. Steel). *SEPM Pacific Section*, 223–231.

Sturdivant A. E. (1988) Uptake of ammonium by potassium-bearing silicates in the Guaymas Basin hydrothermal system, Gulf of California. Master's Thesis, University of California, Riverside, pp. 73.

Sturz A. A. (1991) Experiments on hydrothermal reactions between hemipelagic sediments and seawater. Ph. D. Thesis, University of California at San Diego.

Thompson K. F. (1979) Light hydrocarbons in subsurface sediments. *Geochim. Cosmochim. Acta* **43**, 657–672.

Tissot B. and Welte D. (1984) *Petroleum Formation and Occurrence*, 2nd Edition. Springer Verlag, New York, 699 pp.

Velde B. and Nicot E. (1985) Diagenetic clay mineral composition as a function of pressure, temperature, and chemical activity. *J. Sedimentary Petrol.* **55**, 541–547.

Von Damm K. L., Edmond J. M., Grant B., Measures C. I., Walden B. and Weiss R. (1985) Chemistry of submarine hydrothermal solutions at 21°N East Pacific Rise. *Geochim. Cosmochim. Acta* **49**, 2197–2220.

Von Damm K. L., Edmond J. M., Measures C. I. and Grant B. (1985) Chemistry of submarine hydrothermal solutions at Guaymas Basin Gulf of California. *Geochim. Cosmochim. Acta* **49**, 2221–2237.

Welhan J. A. and Lupton J. E. (1987) Light hydrocarbon gases in Guaymas Basin hydrothermal fluids: thermogenic versus abiogenic origin. *Amer. Assoc. Petrol. Geol. Bull.* **71**, 215–223.

Whelan J. K., Simoneit B. R. T. and Tarafa M. (1988) C_1–C_8 hydrocarbons in sediments from Guaymas Basin, Gulf of California — Comparison to Peru Margin Japan Trench and California Borderlands. *Org. Geochem.* **12**, 171–194.